GEOPHYSICAL APPROACH TO DELINEATE GROUNDWATER POTENTIALS IN THE NORTHWESTERN PART OF WADI DARA, EASTERN DESERT, EGYPT

Aza M. Abdel Rahman*, Fardous. M. Zarif and Ahmed. M. Elshenawy
Department of Geophysical Exploration, Desert Research Center, Cairo, Egypt
*E-mail: azadrc0@gmail.com

The applied geophysical investigations attempt to locate the waterbearing layer(s) that are regarded as the most important elements for the development objectives, which are developed northwest of Wadi Dara, east of the Gulf of Suez. To investigate the condition of groundwater potentials, twenty-five Transients Electromagnetic [TEM] soundings and six two-dimensional Electrical Resistivity Imaging [2D-ERI] lines were conducted. The results of the two geophysical methods detected four main geoelectrical layers (Quaternary alluvium deposits [A], layer of dry sand, gravel and shale [B], waterbearing layer/s [C], and basement rocks [D]). Two aquifers were identified during this study. The first aquifer [sublayer C1] corresponds to sandstone, shale, and limestone deposits of the Middle Miocene age. It has low resistivity values ranging from 3 Ωm to 9 Ωm and is restricted to the east direction. This sublayer had a thickness of about 50 m. The second aquifer [sublayer C2] corresponds to Lower Cretaceous sandstone, which has resistivity values ranging from 13 Ωm to 106 Ωm. It was observed that subsurface geological structures have a significant effect on groundwater occurrences throughout the study area. As a result, the generated geoelectrical cross sections show an apparent connectivity between the two aquifers. Because of variability in resistivity values and thicknesses, the groundwater potential varies throughout the studied area. The western portions of the study areas have priority for drilling productive wells into the lower Cretaceous sandstone aquifer, and then the eastern portions offer groundwater from deposits of sandstone, shale, and limestone of the Middle Miocene age.

Keywords: Wadi Dara, water bearing, electromagnetic, electrical resistivity imaging, aquifers

INTRODUCTION

Egypt is witnessing a rapid expansion in urbanization and population, paralleled by a surge in demand for water resources. The village of Wadi Dara is considered the oldest reclamation society (1989), as well as one of the most promising areas for animal and poultry investment in the Red Sea Governorate (Gomaa et al., 2020). It's on the main road from the inside 10 of paved asphalt. It has several activities, including poultry, olives, palm, jojoba, sheep, and quail farms, as well as tilapia cultivation. Besides, Wadi Dara is one of the migratory birds' stations across the Red Sea. Moreover, the study area is regarded as one of the most active investment zones in the fields of new and renewable energy as well as traditional energy. Despite all these motivating factors, limited water abundance is a prime issue that restricts further development achievements where the majority of previously mentioned activities depend mainly on limited groundwater resources. The investigated area can be classified as hyper-arid. There is no surface water in or nearby the study area. It is crossed by some major wadis, such as Dara, Khurm, Umm Yasar, and Khuraym. Heavy rains in the mountains can cause flash floods in the major wadis.

Groundwater aquifers in the study area and its vicinities can be differentiated into three main layers (Quaternary alluvium, Miocene sandstone, and Lower Cretaceous sandstone) (Gomaa et al., 2020), where only a little water can be stored and collected during rainfall and that can travel over long distances through fissures and pores); groundwater at the alluvial fill of Quaternary age of the Wadis deposits (recharged from occasional rainfall in the mountains and draining fissure water). Water is pumped from deep zones (more than 100 m below the surface) of the Nubian sandstone zone, which are recharged by the existing watersheds in the region. The water is slightly saline (Gomaa et al., 2020). There are no human activities in the study area that use water or cause drainage except the irrigation of the palm trees in the Dara Village and water used by the Bedouin family in the center of the area. The general water supply of the region is from Nile water. A main Nile water pipeline runs parallel to the Suez-Hurghada Road about 6 km from the study area's outer eastern border. The main purpose of establishing the newly reclaimed area around Wadi Dara was to provide job opportunities for the youth and improve their socio-economic status through desert reclamation activities. However, the development and growth of Wadi Dara is currently being stalled, as adequate water resource scarcity is one of the most vital challenges restricting sustainable development in such coastal areas in the arid and semiarid regions.

Development of this area will help in solving the unemployment problems and providing work chances, as the presence of suitable workers in the area will prevent the migration of the workers to Cairo. This will help in solving some of the economic and agricultural problems Egypt is facing. The

aim of the study is to clarify the groundwater occurrences and determine the basement relief in the subsurface. In addition, to investigate the subsurface structures that affect the subsurface sequences and, consequently, the groundwater occurrences in order to find some suitable sites for drilling some production water wells for supplying the area with water for future development processes. The principal objective of this study is to explore groundwater occurrences in its extended surroundings in both north and west directions due to its extensive area, thick alluvium cover, and availability of soil in vast depressions and plains, with the goal of contributing to the growth and expansion of this area. The publications in groundwater techniques are quite limited in the surveyed areas, such as Nasr (1990), Youssef (1992), Helal and Hussein (2015) and Gomaa et al. (2020), but the papers in mineralization exploration are fairly extensive (Bishady et al., 2001; Mostafa and Bishta, 2005; Mahdy et al., 2007 and Gemail et al., 2016).

An integrated geophysical investigation consisting of Transient Electromagnetic [TEM] and two-dimensional Electrical Resistivity Imaging [2D-ERI] was offered in the research region to explore the hydrogeological state of the studied area (Zarif et al. 2021a). A few geophysical investigations have been conducted in the Wadi Dara region (e.g., Helal and Hussein, 2015). These studies are located to the east of the current research and used mostly one-dimensional vertical electrical sounding (1D VES). Since it is particularly sensitive to conductive bodies, TEM has recently become a frequently utilized, inexpensive, and powerful technique in hydrogeological investigation (Sharlov et al., 2019; Killingbeck et al., 2020 and Zarif et al., 2021a). The 2D-ERI approach, on the other hand, is regarded as the first geophysical technique to be intended for locations with limited subsurface data (Dos Santos Gomes et al., 2018; Zarif et al., 2021a and Junaid et al., 2022). Electrical and electromagnetic tools are performed to evaluate groundwater resources because they are both sensitive to physical and chemical variations in the subsurface associated with changing groundwater quality (Louis et al., 2002; Bowling et al., 2007; Rangel et al., 2021 and Zarif et al., 2021b).

Site Characterization

The study area is located in Egypt's North Eastern Desert, in the northwestern portion of Wadi Dara, 47 km south of Ras Gharib and 113 km north of Hurghada (Fig. 1a). The area is located between latitudes 27^{o} 56` 28.55``N and 28$^{o}$ 3` 26.74``N, and longitudes 32^{o} 57` 55.64``E and 33$^{o}$ 15` 14.58``E (Fig. 1b). The study area is classified as a hyper-arid area, with long hot summers, short cold winters, high temperatures, and considerable evaporation, as well as frequent flash floods (Gomaa et al., 2020). Wadi Dara is one of the principal wadis in the Gulf of Suez area, with an oval extended N-S belt of about 28 km in length and an average width of around 25 km, encompassing an area of roughly 700 km^2 (Fig. 1c). Wadi Dara basin has a wavy terrain that progressively slopes eastwards (Fig. 2). The investigated

area has two geomorphic units: highlands (Red Sea mountainous terrain, residual isolated hills, Esh El Mellaha basement ridge, and Shagar tableland) and tectonically regulated morphotectonic depression lands between high mountainous terrain and hilly areas (Abdel Moneim, 2005; Gomaa et al., 2020 and Yousif 2020).

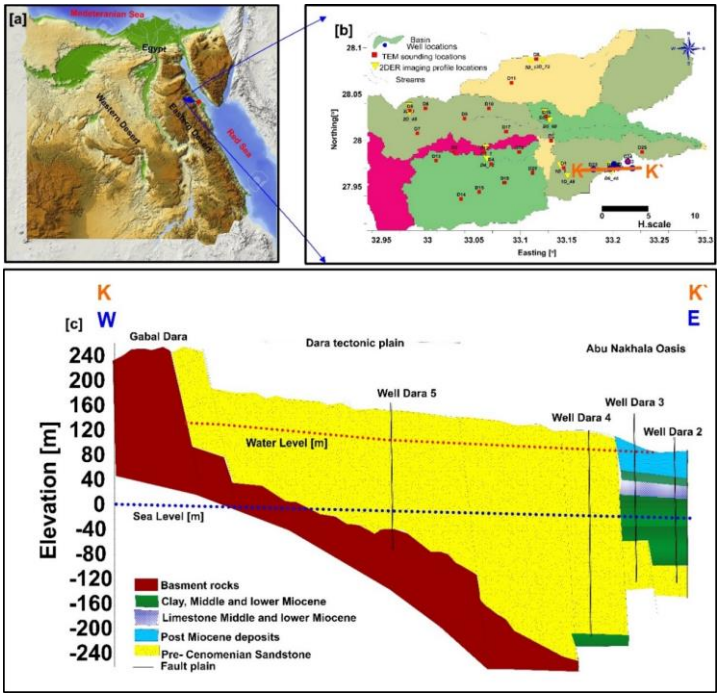

Fig. (1). a. Topographical map for Egypt showing the investigated site. **b.** Digital Elevation map showing location of field work the borders of the study area. **c.** Hydrogeological cross section based on drilled water wells (redraw after Nasr, 1990).

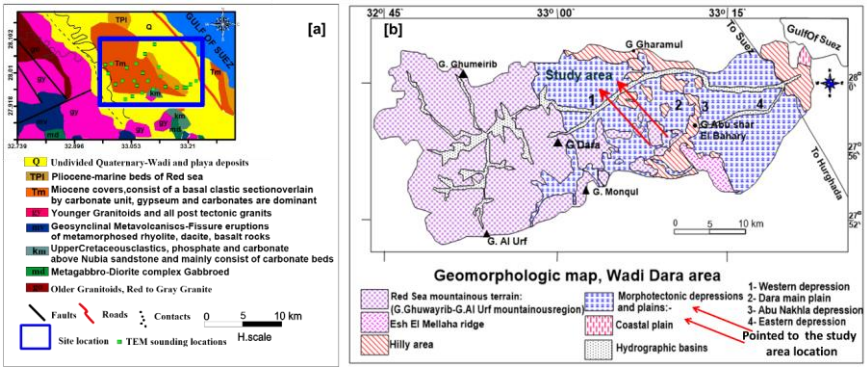

Fig. (2). a. A geological map (after EGPC and CONCO, 1987). **b.** A geomorphological map for the study area (modified after RIGW and ASRT, 2004).

Geologically, Gabel Dara area is characterized by the presence of both igneous and metamorphic rocks of the basement complex, with the exception of its northeastern corner, which is mainly covered by sedimentary rocks (Moustafa and Fouad, 1988). The stratigraphic succession above the basement rocks in the area has developed into different facies, which are dominated by a Paleozoic-Lower Cretaceous sandstone and shale sequence that directly overlies the basement rocks where it dominates the floor of both the western and Dara depressions, and limestone and dolomite in its upper part. On the other hand, several wadis are filled with Pleistocene and Holocene sediments represented by alluvial deposits, fanglomerates, and wadi deposits (Gomaa et al., 2020 and Yousif, 2020). Structurally, normal and strike slip NW- SE and NE - SW faulting are the most dominant trends affecting the study area. They seem to be responsible for groundwater flow from northwest to southeast (especially the former one) and have a direct impact on the hydrogeologic conditions (Yousif, 2020).

The Quaternary alluvium deposits, Miocene sandstone, as well as Lower Cretaceous sandstone aquifers are the main sources of water in the Wadi Dara basin. The Quaternary alluvial is a water-bearing formation downstream of Wadi Dara (east of the Abu Nukhla depression). The groundwater is present in the fractures and cracks of the limestone and marl of the Miocene deposits, where upward leakage from the deep Lower Cretaceous sandstone aquifer and/or fractured Pre-Cambrian rocks is its main source of recharge (Abdel Mohsen et al., 2010 and Elsheikh, 2016). On the other hand, the Lower Cretaceous Nubian sandstone aquifer represents the main source of water in the study area due to its relatively shallow depths and slightly better quality. The hydrochemical analysis results of the three aquifers suggest a hydraulic connectivity between them (Gomaa et al., 2020).

MATERIALS AND METHODS

The methodological approach taken in this study is a mixed methodology based on TEM and 2D-ERI methods. GUPCO, the industrial oil company, and Desert Research Center (Fig. 3) drilled four water wells (Shukair 8, Shukair 9, Dara 4, and Dara 5 wells). These are utilized to calibrate the initial model of both approaches. ZonDTEM1 version 5.1 software was used to interpret TEM soundings measurements where, RES2DINV ver. 3.59.121 software was used to invert the collected 2D-ERI data; and Surfer 13.6.618 (64-bit) (2016) of the Powerful Contouring, Gridding and 3D Surface Mapping Software was used to construct geomorphological, geological, cross-sections and contour maps.

1. Transient Electromagnetic (TEM) Method

The TEM method has been used effectively for groundwater exploration and environmental applications (e.g., Barsukov et al., 2006; Soupios et al., 2015; Kalisperi et al., 2018; Sharlov et al., 2019; Killingbeck

et al., 2020; Zarif et al., 2021a and b). A primary transient current is sent through the transmitter loop in order to produce eddy currents that penetrate deeper into the earth as the interval between pulses increases. High stacking is valuable to get a more realistic curve that is inverted to true resistivity values at different depths. The time interval between turn-off and turn-on switches generally controls the investigated depth, where current intensity gets to greater depths as the time interval increases, and the measured electrical conductivity will depend more on the physical characteristics of deeper layers (Fitterman and Stewart, 1986; McNeill, 1994; Sharma, 1997; Reynolds, 2010 and Kanta et al., 2013). Moreover, the TEM method can resolve the variations of the uppermost layer and offer high quality data compared to other geophysical techniques (Barsukov et al., 2006 and Soupios et al., 2015). TEM_FAST 48 HPC (Version 8) was used to conduct the 1D TEM survey, where the single square loop configuration technique was applied as both transmitter and receiver. A net of 25 TEM soundings of 100 m × 100 m dimension, and 1– 4 Amp current strength, were distributed all over the study area (Fig. 4). The collected TEM data has a calculated root mean square (rms) error of less than 5%. The data were transformed from apparent resistivity change with time (t) to resistivity with depth (z) (Fig. 5) using the TEM-RESEARCHER (TEM-RES-WIN). On the other hand, the ZondTEM1D (version 5.2) was used to transform the collected TEM data to invert an initial model and define the appropriate inversion parameters into the inversion algorithm (Fig. 5). Unfortunately, there are no wells drilled in the study area, however, some information was obtained from the scattered drilled water wells at the north and eastern edges of the study area (Fig. 3) to assume the initial inversion model.

2. Two-Dimensional Electrical Resistivity Imaging (2D-ERI)

The 2D-ERI technique has become the most widely used geophysical method in the field of hydrogeophysics because it provides a measure of the underlying electrical resistivity distribution in both vertical and lateral directions, as well as a more robust and realistic 2D- ERI of the subsurface geological structure and a hydrogeological framework (e.g., Binley et al., 2005, Schrott and Sass 2008, Zarif et al., 2021a and b). The Wenner array layout was used to conduct the 2D-ERI, which involved measuring a number of constant electrodes spacings and increasing the electrode separation with each consecutive datum level. The mathematical and physical principles governing the 2D-ERI technique are discussed in detail in intensive literature (e.g., Dahlin, 2001, Binley et al., 2005, Loke et al., 2013 and Binley, 2015). The 2D-ERI lines distribution were located following the results of the 1D TEM measurements in order to complete the acquired TEM sounding information with the goal of reaching a more realistic subsurface interpretation in both lateral and vertical directions. Across the study area, 6 lines of 2D-ERI Wenner array with electrode spacing of 20 m were performed

(Fig. 6). Data acquisition was performed using Syscal Pro Switch of 10 channels resistivity meter (IRIS Instruments, France) connected to a linear array of 48, 60 and 72 electrodes to achieve the target depth (up to 150 m). In order to get a smoother resistivity and potential distribution and increase solution stability. The Least squares method with regularization was applied using RES2DINV ver. 3.59.121 software to invert the collected 2D-ERI data.

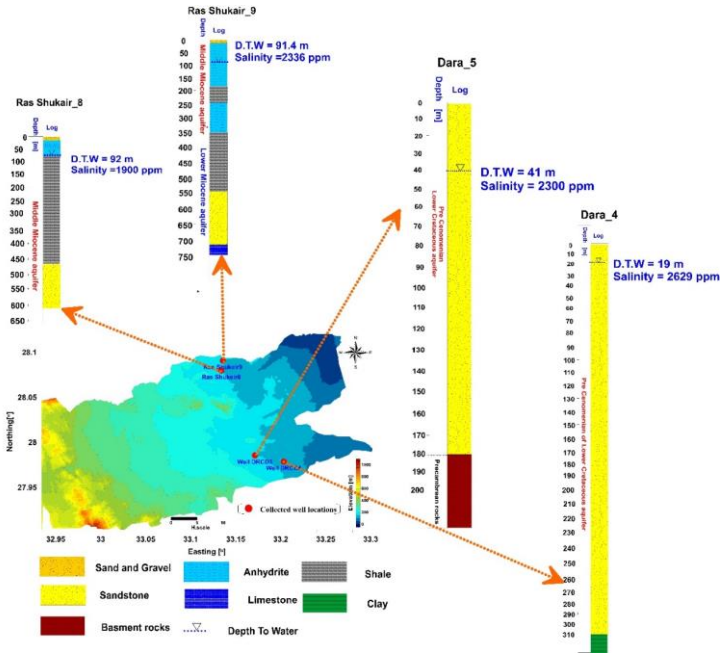

Fig. (3). Available drilled water wells around the investigated area.

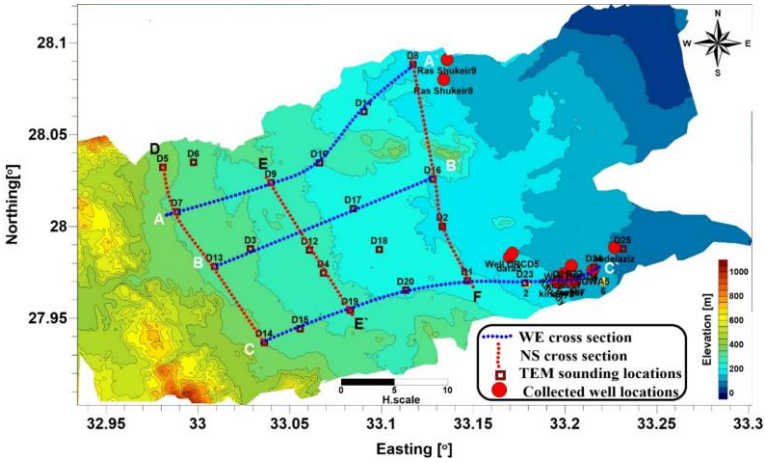

Fig. (4). location map of TEM sounding over investigated sites with SW-NE and NW-SE cross sections.

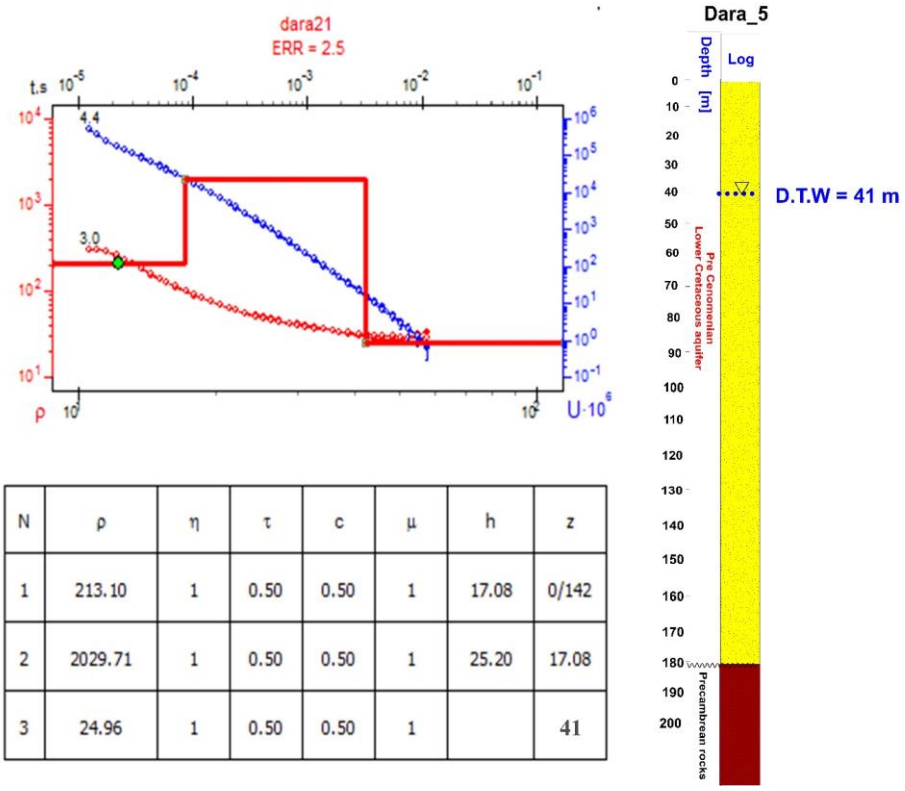

N	ρ	η	τ	c	μ	h	z
1	213.10	1	0.50	0.50	1	17.08	0/142
2	2029.71	1	0.50	0.50	1	25.20	17.08
3	24.96	1	0.50	0.50	1		41

Fig. (5). Analysis of TEM sounding No.21 using ZONDTEM1D software along with the lithologic description of Dara Well 5. (ρ-the resistivity, η polarizability ($0 \leq \eta \leq 1$); c - the exponent; τ - relaxation time, h- Thickness (m) and z-depth to layer).

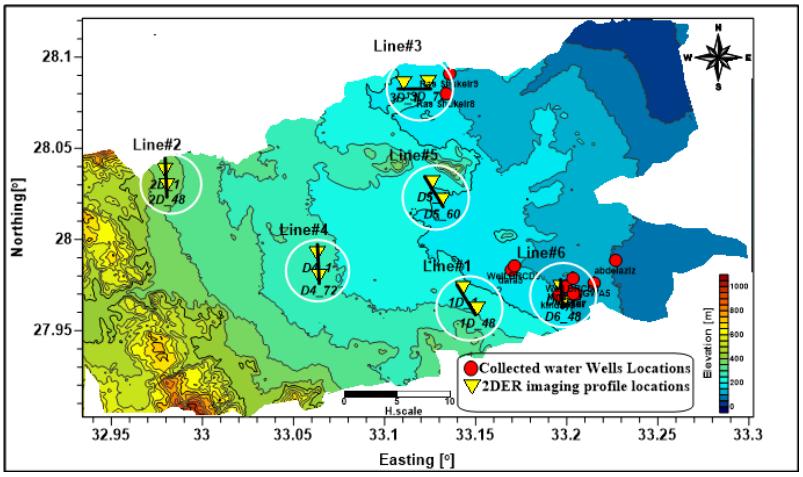

Fig. (6). location map of selected 2D-ERI profiles over the investigated site.

The data quality of the 2D-ERI measurements was evaluated during the current investigation by collecting 338 data sets of reciprocal measurements at line 6, where current and potential dipoles are swapped simultaneously with the normal measurements (LaBrecque et al., 1996; Slater et al., 2000, Koestel et al., 2008 and Zarif et al., 2021a). Depending on the reciprocal error's calculations (ε_R), the acquired 2D-ERI data was filtered, where ε_R< 10 %. The analysis shows that 95 % of the measurements are retained and less than 5 % of the data sets are removed (Fig. 7). This reciprocal error(ε_R) is calculated using PyR2 code (https://gitlab.com/sagitta1618/r2gui/issues).

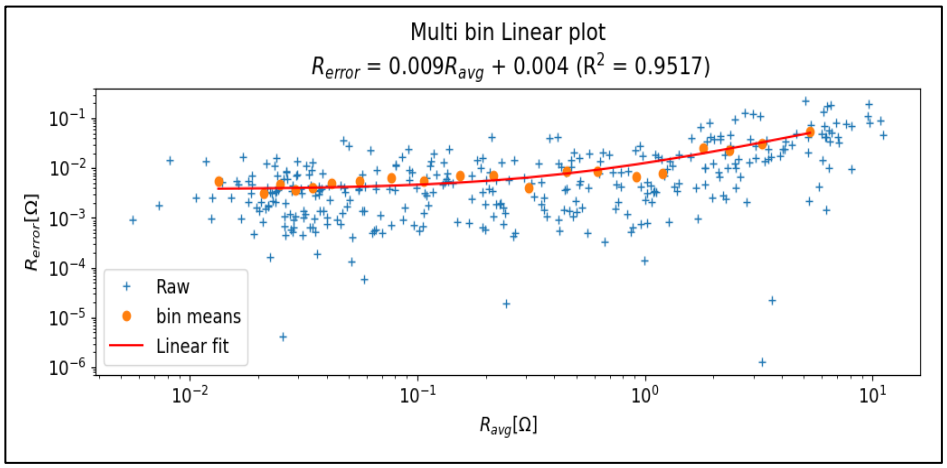

Fig. (7). Error parameters obtained from modeling reciprocal errors (R_{error}) [Ω] of line #6 field data showing orange solid circle represent bins for average of resistance (R_{Avg}) [Ω] magnitude of line #6. Red line represents a power law (Linear) relation to obtain individual resistance error. (PyR2 code, https://gitlab.com/sagitta1618/r2gui/issues).

RESULTS AND DISCUSSION

1. Transient Electromagnetic [TEM]

The interpretation of TEM sounding measurements assists in the construction of six geoelectrical cross sections (A-A', B-B', and C-C` in the SW-NE direction (Fig. 8), D-C, E-E', and A'-F in the NW-SE direction (Fig. 9). These sections illustrate the geoelectrical sequence, lateral and vertical resistivities that reflect the lithology changes of the different layers and the subsurface structures along the profile directions.

Fig. (8) depicts the condition of the hydrogeology of the study area based on inverted resistivity and thickness values in vertical and horizontal directions along SW-NE cross-sections with the distribution of subsurface lithological composition related to the geological and hydrogeological background of the investigated site. The geoelectrical succession of the area under study consists of a number of layers, grouped together in four main

geoelectrical layers. The first layer (surface layer A) is composed of sand, gravel and clay corresponding to Alluvium wadi deposits. The second layer [B] is composed of dry sand and gravel, third layer [C] which is subdivided into two sublayers that correspond to Middle Miocene aquifer [sublayer C1] and lower cretaceous sandstone deposits [sublayer C2] and the last layer D is the Precambrian basement rock (Table 1).

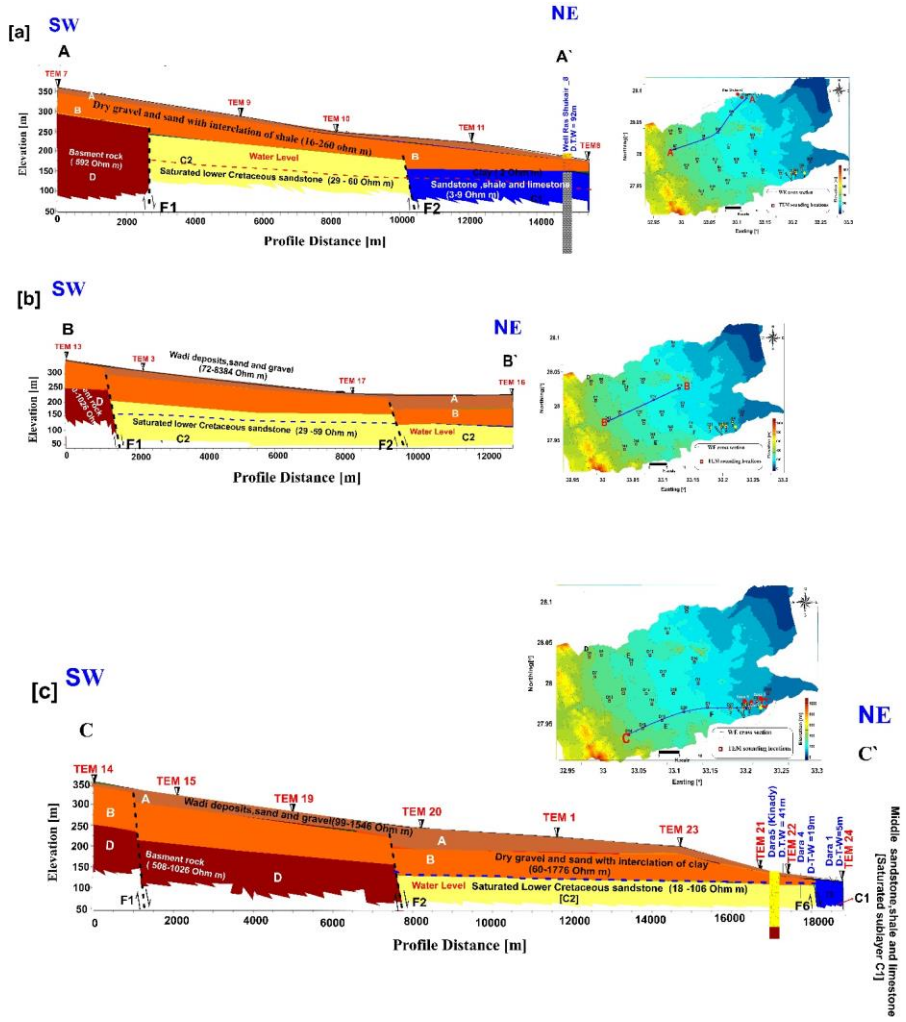

Fig. (8). Geoelectrical cross sections in SW- NE direction of the investigated area. **a.** geoelectrical cross section A-A`. **b.** geoelectrical cross section B-B`. **c.** geoelectrical cross section C-C` in the north, middle and south parts of study area, respectively.

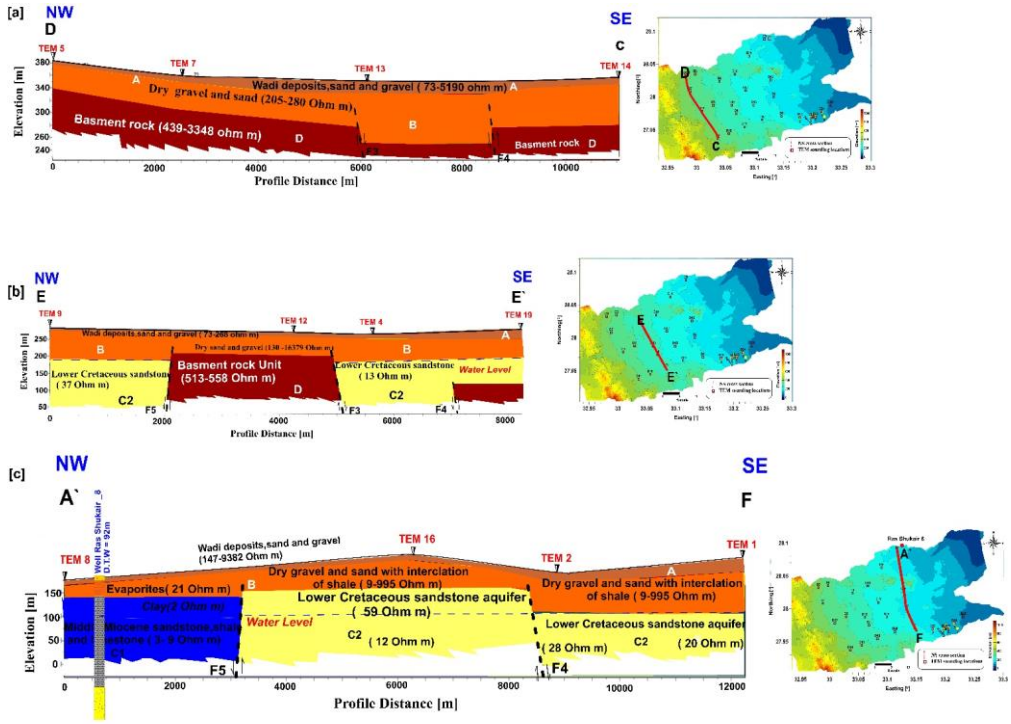

Fig. (9). Geoelectrical cross sections in NW- SE direction in the investigated area. **a.** geoelectrical cross section D-C. **b.** geoelectrical cross section E-E`. **c.** geoelectrical cross section A`-F in the west, middle and east parts of study area, respectively.

Table (1). A summary of resistivity and thickness of the geoelectrical layers as well as their lithological description:

Layer ID	Sublayer	Resistivity [Ωm] (min-max)	Thickness [m] (min-max)	Lithological Description
Layer A		72 -8384	0.5-28	Quaternary Alluvium deposits
Layer B		9-16379	1 -147	Dry Sand, Gravel and Shale
Layer C	**Sublayer C1**	3- 9	----------	Middle Miocene sandstone, shale and limestone deposits (Waterbearing)
	Sublayer C2	13 -106	~50	Lower Cretaceous sandstone (waterbearing)
Layer D		508 - 3348	----------	Precambrian Basement Rocks

The first layer consists of combining the thinnest upper layers with the lowest main layer. To obtain a single resistivity value for these thin layers, the transverse resistivity (ρ_t) should be estimated from the resistivities and thicknesses of the thin layers as follows:

$$\rho_t = \sum(\rho_i h_i)/\sum h_i \quad \text{.....} i=1 \text{ to } n \quad [1]$$

Where; (ρ_i) is the resistivity of the (ith) layer, (h_i) is its thickness, and n is the number of layers.

The equivalent resistivity and thickness of this layer have resistivity values ranging between 72 Ωm and 8384 Ωm. The low resistivity value corresponds to the clayey sand deposits of Quaternary alluvium, whereas the high resistivity is related to dry sands, gravel, and sandstone of Quaternary age. The thickness of this layer varies from 0.5 m to 28 m. The second geoelectrical layer [B] has resistivity values varying from 9 Ωm to 16379 Ωm. The resistivity values of this layer corresponds to a dry sandstone, fragment rocks, and gravel with intercalation of shale deposits as shown along the E-E` cross section (Fig. 9b). The thickness of this geoelectrical layer ranges between 1 m and 147 m.

The resistivity values of the third geoelectrical layer [C] range from 3 to 106 Ωm (Table 1). This layer is subdivided into two sublayer C1 and C2 which are corresponding to the deposits of Middle Miocene aquifer and Lower Cretaceous aquifer, respectively. Geoelectrical sublayer [C1] has resistivity values varying from 3 Ωm to 9 Ωm. It represents the Middle Miocene aquifer of sandstone, shale and limestone. Because of the high clay content in the sandstone of the middle Miocene deposits, the resistivity values of this geoelectrical sublayer usually decreases eastward the downstream of wadi Dara (Fig. 9c) and hence, effect on the quality of groundwater particularly, east and northeast portion of the study area. The depth of this layer varies from 93 m to 140 m. This geoelectrical layer was only detected at TEM sounding nos. 11, 16, 18, 24, and 25.

A lower Cretaceous sandstone aquifer [sublayer C2] with relatively high resistivity values (13-106 Ωm) was detected along all cross sections under the majority of TEM soundings except at TEM soundings along cross section D-C (Fig. 9a). This sublayer [C2] is considered the main waterbearing formation at the western part of the study area. The bottom of this layer was undiscovered by the applied techniques used, and there is no independent subsurface lithological information at these locations. On the other hand, [C2] doesn't detected at some locations (TEM 5, TEM 7, TEM 12, TEM 13, TEM 14, TEM 15 and TEM 19), where the extremely high resistivity values of basement rock layer [D] is directly recorded beneath the geoelectric layer [B] (Fig. 9a).

Fig. (10a) shows the iso resistivity contour map of the main waterbearing layers [sublayer C1 and sublayer C2], demonstrating that resistivity values of sublayer [C2] (Lower cretaceous aquifer) increases

towards the west and southwest of the study area and has a relatively higher resistivity than sublayer [C1] of the Middle Miocene aquifer which decreases towards the east and northeast of Wadi Dara. Depth to waterbearing layers [C1 and C2] is demonstrated in Fig. (10b). The maximum depth is estimated at TEM 18 and 20 where the minimum one is recorded at TEM 24.

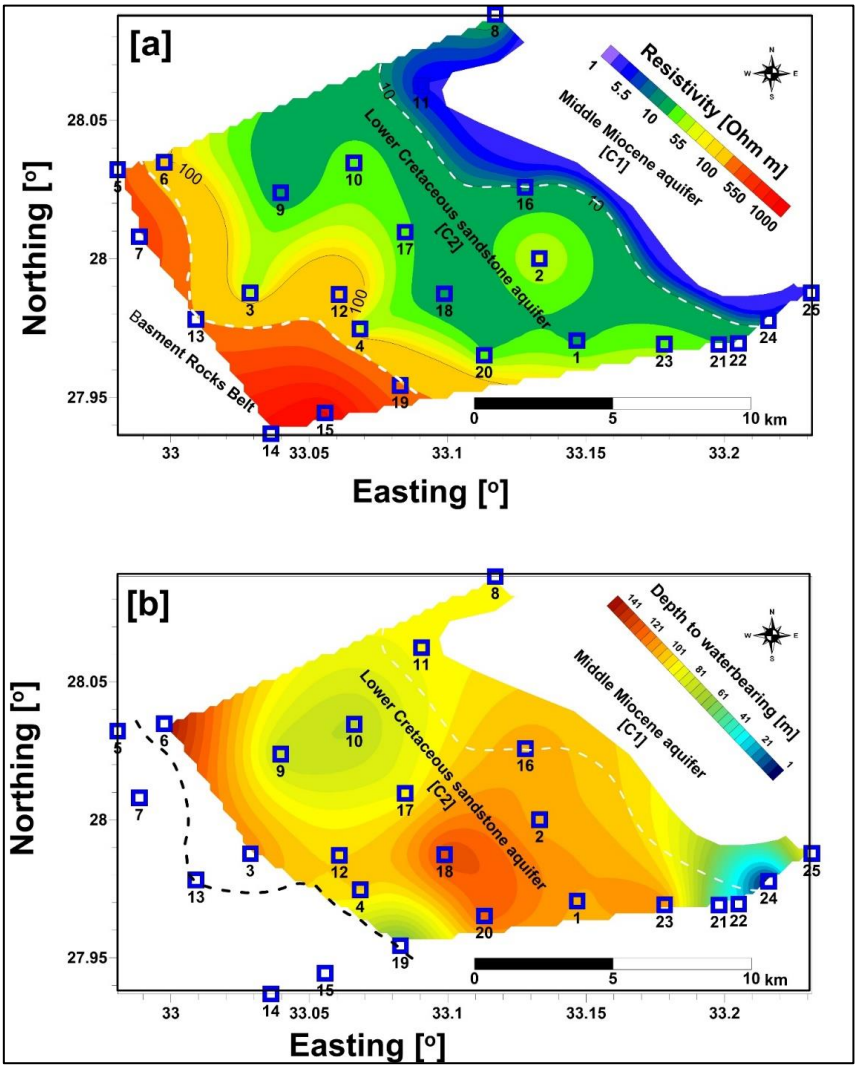

Fig. (10). a. Iso resistivity contour map of waterbearing layers [C1 and C2]. **b.** Depth contour map of main waterbearing layers [C1 and C2]. Blue squares representing the location of TEM sounding measurements.

Fig. (11) demonstrated the detected lineament structures (F1: F6) based on the interpretation of TEM sounding results. These lineaments (faults) have a significant role in groundwater potential because they improve water

movement and aquifer storage. The figure also includes the shallow and deep-seated lineament structure, which were extracted by Gemail et al. (2016) as regional and residual magnetic components from the analysis of aeromagnetic data of the western side of the study area, respectively, which matches well with the resulting lineament structure from TEM interpretation. According to the extracted lineament structure, the main faulting trends affecting the study area are NW-SE, E-W, NNW-SSE, and N-S, with minor faulting trends in NE-SW and NNE-SSW (Gemail et al., 2016).

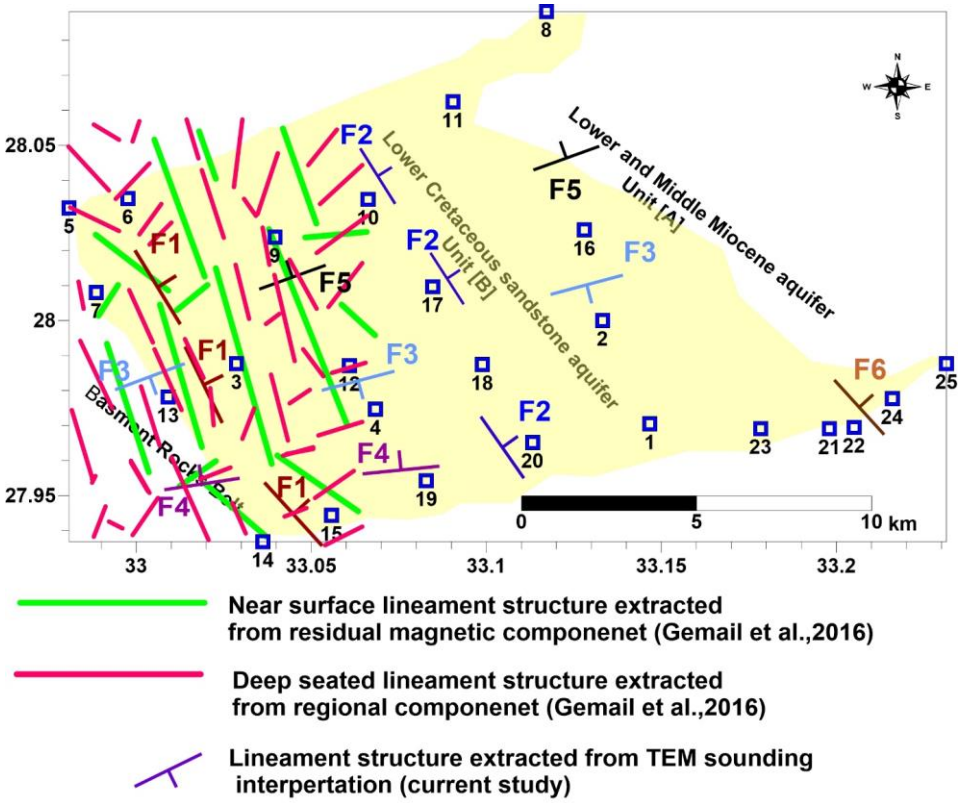

Fig. (11). Deduced structure map based on the results of previous work (Gemail et al., 2016) and the current study, blue squares representing the location of TEM sounding measurements.

2. 2D Electrical Resistivity Imaging Data [2D-ERI]

A forward modelling subroutine was used to calculate the apparent resistivity values, where a non-linear least square optimization technique is used for the inversion routine (Griffiths and Barker, 1993; Loke and Barker, 1996). According to the resistivity values along the resistivity model, the actual resistivity plot of the 2D-ERI of line #1 at the downstream of Wadi

Dara (Fig. 12a) shows that this model comprises of three layers. The uppermost layer is mainly dry [A], with a resistivity range of 3348 to more than 14000 Ωm. The thickness of this layer reaches 40 m along the whole line. The second layer [B] represents the layer of dry sand and gravel. It consists of a group of thin layers whose resistivity decreases downward from about 3348 Ωm to about 250 Ωm. This layer extends from a depth of 40 m to about 100 m. The waterbearing formation (Lower cretaceous sandstone aquifer) is represented by the third lower layer [C2] in the geoelectrical cross section C-C` of TEM 1 (Fig. 8c). The interpreted results of line #1 indicate that this site is classified as of high potential groundwater where the depth to the lower cretaceous sandstone sublayer [C2] waterbearing is ~ 100 m. The inverted resistivity model of line #2 in the northwestern part of the study area (Fig. 12b) shows three resistivity layers. The top layer is alluvium wadi deposits [A], with resistivity values ranging from 1.0 Ωm to more than 14059 Ωm. This layer has a thickness of roughly 17 m. The intermediate layer represents a layer of dry lower cretaceous sandstone deposits [B], with resistivity ranging from around 250 to 1634 Ωm. It has an average depth of 40 m. The last layer is characterized by steadily increase of resistivity corresponding to the basement rocks layer [D]. The resistivity value of this layer is more than 14059 Ωm. The potentiality of this site is classified as poor where the area is so close to basement outcrops and overlain sedimentary deposits are dry (250 to 3348 Ωm).

Fig. (12c) depicts the inverted resistivity model of line #3 in the northeastern corner of the study area. This 2D-ERI line passes via TEM 8, which is considered a part from cross section A`- F, where the observations of this line coincide well with the interpretation of the TEM 8 (Fig. 9c). The groundwater potentiality as this part of the study area is considered high, where saline Middle Miocene aquifer is the main source of water for industrial purposes (Ras Shukair oil site).

The 2D-ERI of line #4 exhibits the same characteristics as that of line #2 (Fig. 12d), except this line is passed by TEM 12. The uppermost layer [A] has a wider range of resistivity values (50 to 14000 Ωm). This might be associated with dry Quaternary alluvium deposits. This layer has a thickness ranging from 25 to 50 m. The second layer [B] which is represented by dry sand, gravel and sandstone of resistivity values varies between (250 and 797 Ωm). This layer is directly followed by a highly resistive layer, which is mainly attributable to Precambrian basement rocks [D]. Groundwater

potential along this line is poor where the overlain sedimentary layers is very resistive, as shown in Fig. (12d).

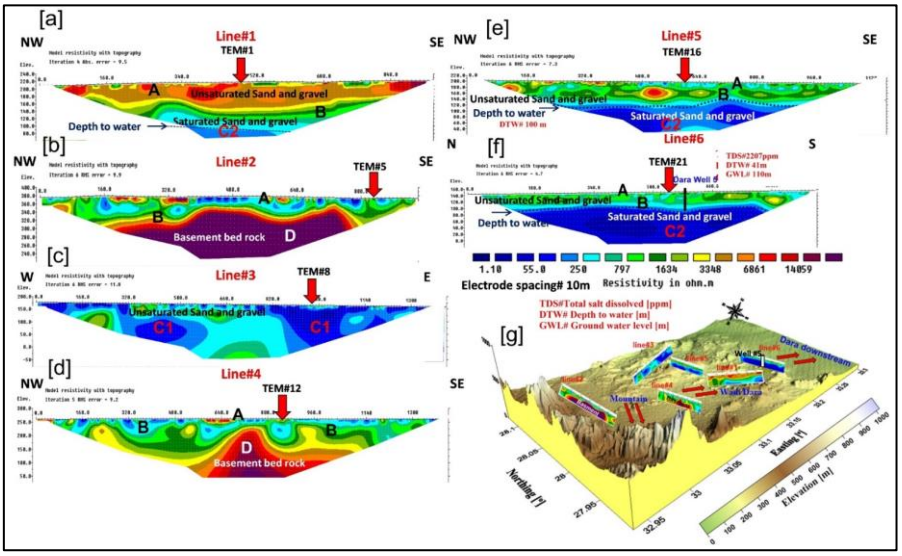

Fig. (12). Inversion models for six 2D-ERI lines distributed over the topographic map. **a.** line #1, **b.** Line #2, **c.** line #3, **d.** Line #4, **e.** Line #5, **f.** Line #6, **g.** over the investigated area.

The 2D inverted resistivity models of lines #5 and #6 (Fig. 12e and f) reveal that the resistivity values vary laterally and vertically, indicating three geoelectrical layers. TEM 16 is positioned at line #5 (Fig. 12e), at a lateral distance of 560 m, whereas TEM 21 is located at a lateral distance of 540 m along line #6 (Fig. 12f). The uppermost layer [A] of high resistivity values (250-14000 Ωm) showed inhomogeneous sand and gravel deposits, where the second layer [B] represents the layer of dry lower cretaceous sandstone and is immediately overlaid by the saturated layer of lower Cretaceous sandstone [C2]. The thickness of this layer varies along the two lines. The thickness of the dry layer at line #5 ranges from 80 to 100 m, whereas at line #6 it ranges from 38 to 42 m. The waterbearing resistivity layer ranges between 5 and 55 Ωm at the two lines. This low resistivity may be related to increases in clay content and salinity, particularly near the Dara basin's outflow (Salinity= 2629 ppm). The findings of the 2D-ERI lines support the interpretation of the TEM sounding data. Fig. (12f) depicts the location of Dara Well 5 at 2D-ERI of line #6. This well is very necessary for the calibrating and interpreting of the 2D-ERI data. The depth to water is estimated to be 100 m along line #5. On the other hand, the depth to water at line #6 is 41 m, which corresponds to the description of well Dara 5. The results show the existence of two waterbearing layers inferred as the potential groundwater recharge sublayers (C1 and C2), which are separated by vertical geological structure in the study area Fig.

(12g). The groundwater potential at the two sites of lines 5 and 6 is considered good, particularly for sustainable development in the future.

3. Groundwater Occurrences

The Middle Miocene sandstone, shale, and limestone deposits (geoelectrical sublayer C1) and Lower Cretaceous sandstone (geoelectrical sublayer C2) are the waterbearing zones in the study area. The Middle Miocene aquifer is recorded in the eastern and northeastern parts of the Wadi Dara and Ras Shukair outlets. It is made mostly of sandstone, shale, limestone, and, in some places east of Dara downstream, evaporite deposits (Moustafa and Fouad,1988).

The lower Cretaceous sandstone, on the other hand, is found west, northwest, and southwest of Wadi Dara and is formed of sandstone intercalated with clay. A fault system is inferred from hydrogeophysical studies and shows that there is a connection between the two waterbearing zones. They may be capable of supplying each other through this possible connection. The interpreted electromagnetic data shows that the depths to the top of sublayer C1 range from 1.5 m in the east (TEM 24) to 92 m in the north (TEM 8), whereas the depths to the tops of sublayer C2 range from 76 m to 150 m at TEM 6 (Fig. 10b). The water level of this layer ranges from 1 m in the east (TEM 24) to 136 m in the west (TEM 18). As a result, groundwater flows regionally from west to east.

The resistivity values of the electromagnetic sublayer (C1) range from 3 Ωm in the east to 9 Ωm in the northwest, where sublayer (C2) provides a higher resistivity range [13-106 Ωm], evidencing that the western portion of the studied area has better water quality (lower cretaceous sandstone aquifer). Furthermore, the relative quality of groundwater declines eastward due to an increase in clay content and/or salinity (2629 ppm). The waterbearing layers in the studied area are mostly constituted of sedimentary succession overlaying Precambrian basement rocks. These successions contain Lower Cretaceous sandstone, Middle sandstone, shale and limestone overlain by dry sand, gravel, and Quaternary Wadi alluvium deposits. Moreover, the studied area was dissected by many faults found by TEM sounding interpretation (F1:F6), and these findings are consistent with those of Gemail et al. (2016).

CONCLUSIONS

Twenty-five Transient Electromagnetic soundings [TEM] and six lines of 2D electrical Resistivity Imaging [2D-ERI] were conducted in this study to clarify the hydrogeophysical condition of the investigated area. Four subsurface geoelectrical layers (alluvium deposits layer, dry sand, gravel, and shale, waterbearing and basement rocks) were detected. The depth to waterbearing zones in Wadi Dara ranges from 1.5 m in the east to 150 m in the northwestern part. The main aquifer in the study area is the sandstone of lower Cretaceous age, while the other one is the Middle Miocene aquifer,

which is restricted only to the northeastern, and eastern parts of Wadi Dara. The quality of groundwater in the investigated area is related to the estimated true resistivity, which increases towards the western and northwestern parts of Wadi Dara and decreases towards the eastern parts, where the shale content and salinity increase.

The area under investigation is affected by a number of normal faults trending NW-SE, E-W, and N-S directions. It is highly recommended to use Magnetotellurics (MT) in such areas to investigate the whole thickness of the lower cretaceous sandstone (C2) aquifer. Besides, regarding the distance between the future wells, the distance in-between two successive wells should be 500 m. Also, a buffer of less than 500 m should be considered around the fault location for drilling new water wells. Finally, the findings of the current study hope to provide small and big investors, as well as decision makers, with the favorable locations and hydrogeological conditions for agricultural, animal, and poultry investment development in order to secure food, establish urban communities, and create job opportunities for the youth sector, aiming to improve their socio-economic status through desert reclamation activities.

REFERENCES

Abdel Mohsen, H.M., A.A. Tarek and R. Ashraf (2010). New lights on the hydrogeology of Wadi Dara, Western side of the Gulf of Suez Egypt. Sedimentol Egypt, 18: 131–146.

Abdel Moneim, A.A. (2005) Overview of the geomorphological and hydrogeological characteristics of the Eastern Desert of Egypt. Hydrogeology Journal, 13 (2): 416–425.

Barsukov, P.O., E.B. Fainberg and E.O. Khabensky (2006). Shallow Investigation by TEM FAST Technique: Methodology and Case Histories. In: "Methods of Geochemistry and Geophysics", Spichak, V.V. (Ed.), 40: 55–77.

Binley, A. (2015). DC Electrical Methods. In: "Treatise on Geophysics". Elsevier, pp. 233-259. https://doi.org/10.1016/B978-0-444-53802-4.00192-5.

Binley, A., A. Kemna, Y. Rubin and S. Hubbard (2005). DC Resistivity and Induced Polarization Methods. Hydrogeophysics, Springer, pp. 129–156. https://doi.org/10.1007/1-4020-3102-5_5

Bishady, A.M, M.H. Shalaby, H.A. Eliwa and M.I. Bassuoni (2001). Mineralogical and geochemical studies on the copper mineralized rocks of Wadi Dara area, North Eastern Desert, Egypt. Al-Azhar Bull. Sci., Proc. 4th Int. Sci. Conf. (March, 2001): 393-430.

Bowling, J.C., D.L. Harry, A.B. Rodriguez and C. Zheng (2007). Integrated geophysical and geological investigation of a heterogeneous fluvial aquifer in Columbus Mississippi. J. Appl. Geophys., 62: 58–73.

Dahlin, T. (2001). The development of DC resistivity imaging techniques. Computers Geosciences, 27 (9): 1019–1029.

Dos Santos Gomes, J. L., F.P. Vieira and V.M. Hamza (2018). Use of electrical resistivity tomography in selection of sites for underground dams in a semiarid region in southeastern Brazil. Groundwater for Sustainable Development, 7 (1): 232–238.

EGPC (Egyptian General Petroleum Corporation) and CONCO (1987). A geo- logical map of Egypt, 1: 500000, 20 sheets (Bani Suef Assiut and South Sinai sheets).

Elsheikh, A. (2016). Management of water resources in wadi dara area using mathematical modeling for sustainable development, eastern desert Egypt. Egypt. J. Geol., 60: 37–59.

Fitterman, D.V. and M.T. Stewart (1986). Transient electromagnetic sounding for groundwate. Geophysics, 51: 995–1005.

Gemail, K., N.M. Abd-El Rahman, B.M. Ghiath and R.N. Aziz (2016). Integration of ASTER and airborne geophysical data for mineral exploration and environmental mapping: a case study, Gabal Dara, North Eastern Desert, Egypt. Environmental Earth Sciences, 75 (7). https://doi.org/10.1007/s12665-016-5368-0.

Gomaa, M.A., A.R. Shabana and E. Zaghlool (2020). New approach in sustainable development based on groundwater resources, Wadi Dara, Eastern Desert, Egypt. Environmental Earth Sciences, 79 (13): 1-20.

Griffiths, D.H. and R.D. Barker (1993). Two- dimensional resistivity imaging in areas of complex geology. Journal of Applied Geophysics, 29: 211-226.

Helal, S.A. and A.W. Hussein (2015). Utilization of hydrogeophysics in assessment of the groudwater Aquifer at Wadi Dara area, Eastern Desert, Egypt. Eighth International Conference on the Geology of Africa p-p vii-27 - vii-54 (Nov. 2015) Assiut, Egypt. 54 (1979): 13–25.

Junaid, M., R.A. Abdullah, R. Sa'ari et al. (2022). Water-saturated zone recognition using integrated 2D electrical resistivity tomography, borehole, and aerial photogrammetry in granite deposit, Malaysia. Arabian Journal of Geophysics, 15 (14): 1301.

Kalisperi, D., M. Kouli, F. Vallianatos, P. Soupios, S. Kershaw and N. Lydakis-Simantiris (2018). A transient electromagnetic (TEM) method survey in north-central coast of crete, Greece: Evidence of seawater intrusion. Geosciences (Switzerland), 8 (4). https://doi.org/10.3390/geosciences8040107.

Kanta, A., P. Soupios, P. Barsukov, M. Kouli and F. Vallianatos (2013). Aquifer characterization using shallow geophysics in the keritis basin of western crete, Greece. Environmental Earth Sciences, 70 (5): 2153-2165.

Killingbeck, S.F., A.D. Booth, P.W. Livermore, C. Richard Bates and L.J. West (2020). Characterisation of subglacial water using a constrained

transdimensional Bayesian transient electromagnetic inversion. Solid Earth, 11 (1): 75–94.

Koestel, J., A. Kemna, M. Javaux, A. Binley and H. Vereecken (2008). Quantitative imaging of solute transport in an unsaturated and undisturbed soil monolith with 3D ERT and TDR. Water Resources Research, 44 (W12411). https://doi.org/10.1029/2007WR006755.

LaBrecque, D.J., M. Miletto, W. Daily, A. Ramirez and E. Owen (1996). The effects of noise on Occam's inversion of resistivity tomography data. Geophysics, 61: 538–54.

Loke, M.H. and R.D. Barker (1996). Rapid least squares inversion of apparent resistivity pseudosections by a quasi-Newton method. Geophys. Prospect, 44: 131–152.

Loke, M.H., J.E. Chambers, D.F. Rucker, O. Kuras and P.B. Wilkinson (2013). Recent developments in the direct-current geoelectrical imaging method. J. Appl. Geophys., 95: 135-156.

Louis, I.F., F.I. Louis and A Grambas (2002). Exploring for favorable groundwater conditions in hard rock environments by resistivity imaging methods: synthetic simulation approach and case study example. International Conference on Earth Sciences and Electronics (ICESE-2002). Journal of Electrical &Electronics Engineering. Special Issue, October 2002, pp. 1–15.

Mahdy, A.I., M.M. El-sankary and M.H. Shalaby (2007). Gamma-ray spectrometry and mineralogical characteristics of Wadi Dara Cu-mineralization, North Eastern Desert. Egypt. J. Appl. Geophys., 6 (1): 1-20.

McNeill, J.D. (1994). Principles and Application of Time Domain Electromagnetic Techniques for Resistivity Sounding. Technical Note TN-27, Geonics Ltd., Ontario.

Mostafa, M.E. and A.Z. Bishta (2005). Significance of lineament patterns in rock unit classification and designation: A pilot study on the Gharib-Dara area, northern Eastern Desert, Egypt. International Journal of Remote Sensing, 26 (7): 1463–1475.

Moustafa, A.R. and H.G. Fouda (1988). Gebel Sufr El Dara Accommodation Zone, Southwestern Part of the Suez Rift: M.E.R.C. Ain Shams Univ. Earth Sci. Ser., 2: 227-239.

Nasr, M.I. (1990). Geological and geophysical studies on groundwater potentialities in the area between Ras Gharib and Ras Gemsa. MSc. Thesis, Faculty of Science, Al Azhar Univ., Egypt.

Rangel, R.C., A.D. Parsekian, L.M. Farquharson, B.M. Jones, N. Ohara, A.L. Creighton, B.V. Gaglioti, M. Kanevskiy, A.L. Breen, H. Bergstedt, V.E. Romanovsky and K.M. Hinkel (2021). Geophysical observations of Taliks below drained lake basins on the arctic coastal plain of Alaska. Journal of Geophysical Research: Solid Earth, 126 (3). https://doi.org/10.1029/2020JB020889.

Reynolds, J.M. (2010). In: "An Introduction to Applied and Environmental Geophysics". In preparation due to 2010. John Willey and Sons, USA.

RIGW and ASRT (2004). Research Institute for Groundwater and Academy of Scientific Research and Technology Groundwater Potentiality Maps, 2004, Internal Report Submitted to Academy Scientific Research, Cairo, Egypt.

Schrott, L. and O. Sass (2008). Application of field geophysics in geomorphology: Advances and limitations exemplified by case studies. Geomorphology, 93 (1–2): 55–73. https://doi.org/10.1016/j.geomorph.2006.12.024.

Sharlov, M., I. Buddo, A. Pisarnitskiy, N. Misurkeeva and I. Shelohov (2019). Shallow transient electromagnetic method application for groundwater exploration: case study from Greece. ASEG Extended Abstracts, 2019 (1): 1–5.

Sharma, P. (1997). In: "Environmental and Engineering Geophysics". Cambridge University press, UK.

Slater, L., A. Binley, W. Daily and R. Johnson (2000). Cross-hole ERT imaging of a controlled tracer injection. J. Appl. Geophys., 44: 85-102.

Soupios, P., K. Nektarios, D. Zoi, K. George, P. George, V. Antonis and M. Emmanuil (2015). Modeling saltwater intrusion at an agricultural coastal area using geophysical methods and the FEFLOW model. In: "Engineering Geology for Society and Territory", vol. 3. Lollino, G.; M. Arattano, M. Rinaldi et al. (Eds.). Springer, Cham, Switzerland, pp. 249-252.

Yousif, M. (2020). Combination of remote sensing, GIS and palaeohydrologic remarks for promoting the exploitation of water resources in the Sahara: cases from the Red Sea Coast, Egypt. In Environmental Earth Sciences, 79 (10). https://doi.org/10.1007/s12665-020-08977-6.

Youssef, A.M. (1992). Application of geographic information systems (G.I.S) in geophysical and sedimentological studies for groundwater potentialities in Ras Garib area, Egypt. MSc. Thesis, Faculty of Science, Ain Shams Univ., Egypt.

Zarif, F.M., A.M. Elshenawy and M.A. Mabrouk (2021a). Integrated TEM and 2DERI techniques to delineate groundwater bearing zones in fractured carbonate rocks at the upstream portion of wadi Halazeen, Northwestern Coast, Egypt. Journal of African Earth Sciences, 182 (2021): 104288.

Zarif, F., H. Isawi, A. Elshenawy and M. Eissa (2021b). Coupled geophysical and geochemical approach to detect the factors affecting the groundwater salinity in coastal aquifer at the area between Ras Sudr and Ras Matarma area, South Sinai, Egypt. Groundwater for Sustainable Development, 100662. https://doi.org/10.1016/J.GSD.2021.100662.

نهج جيوفيزيائي لتحديد إمكانيات المياه الجوفية في الجزء الشمالي الغربي من وادي دارا، الصحراء الشرقية، مصر

عزة محمد علي*، فردوس محمد ظريف وأحمد محمد الشناوي
قسم الإستكشاف الجيوفيزيائي، مركز بحوث الصحراء، القاهرة، مصر

تم إجراء المسوحات الجيوفيزيائية التطبيقية بهدف تحديد الطبقة أو الطبقات الحاملة للمياه الجوفية والتي تعتبر من أهم العناصر لتحقيق أهداف التنمية المستدامة بمنطقة الدراسة التي تقع شمال غرب وادي دارا - شرق خليج السويس. تم إجراء خمسة وعشرون جسة كهرومغناطيسية وستة بروفيلات من القطاعات الجيوكهربية الثنائية الأبعاد لمعرفة ظروف تواجد المياه الجوفية بمنطقة الدراسة. من تفسير البيانات الكهرومغناطيسية والجيوكهربية تم تحديد أربع طبقات أساسية: الطبقة الأولى (A) طبقة سطحية من رواسب الوديان، الطبقة الثانية (B) طبقة جافة من الحصى والرمال، والطبقة الثالثة (C) هي الطبقة الحاملة للمياه الجوفية وتنقسم إلي طبقتين فرعيتين، الأولى (C1) والثانية (C2)، الطبقة الفرعية الأولي (C1) تتوافق مع رواسب الحجر الرملي والطين والحجر الجيري التابع للعصر الميوسيني الأوسط، بينما الطبقة الفرعية الثانية (C2) تتوافق مع الحجر الرملي التابع للعصر الطباشيري السفلي، وأخيرًا الطبقة الرابعة (D) وهي طبقة صخور القاعدة. تتراوح المقاومة الكهربية النوعية للطبقة (C1) من ٣ أوم. متر إلى ٩ أوم. متر وتتركز بمنطقة الشرق والشمال الشرقي ويصل سمكها في بعض الأماكن إلى ٥٠ متر في حين تتراوح المقاومة الكهربية النوعية للطبقة (C2) ما بين ١٣ أوم. متر و١١٦ أوم. متر وتقع في المنطقة الغربية للدراسة. فالمقاومات المنخفضة (١٣ أوم. متر) ترجع إلى وجود تداخلات من رواسب الطين في التكوين الرسوبي، والمقاومات العالية (١١٦ أوم. متر) ترجع إلى وجود رواسب الرمال والحجر الرملي النوبي. بالإضافة إلى ذلك، وجد أن التراكيب الجيولوجية تحت السطحية لها تأثير كبير في ظروف تواجد المياه الجوفية بمنطقة الدراسة كما هو واضح من القطاعات الجيوكهربية. ونظرًا للإختلاف في قيم المقاومة الكهربية النوعية وسمك الطبقات الحاملة للمياه الجوفية، وجد أن هناك تباين كمي ونوعي بخصائص الخزانات الجوفية بالمنطقة حيث تتمتع المناطق الغربية من منطقة الدراسة بالأولوية في حفر الآبار المنتجة من طبقة الحجر الرملي النوبي التابع للعصر الطباشيري السفلي، ثم يليها الأجزاء الشرقية من رواسب الحجر الرملي الميوسيني الأوسط، وحفاظًا على الآبار المستقبلية وعلى عدم تدهور الخزان الجوفي فإنه يجب تجنب الحفر العشوائي وأن تختار بدقة مواقع الآبار المستقبلية الجديدة مع مراعاة المسافة بين الآبار بعضها البعض وكذلك المسافة بين الآبار وبين التراكيب الجيولوجية المؤثرة على التتابع الصخري وعلى تواجد المياه الجوفية بحيث تكون المسافة بين البئر والصدع المؤثر على الطبقات لا تقل عن ٥٠٠ متر. وأخيرًا يجب إستخدام الري بالتنقيط مع عمل نظام صرف جيد لتجنب مشكلة غدق التربة وذلك لوجود طبقات الطين قريبة من السطح، كل ذلك يفيد في توعية المستثمرين بتجنبهم إستخدام السحب العشوائي الذي يعمل على تدهور الخزان الجوفي وزيادة ملوحته وتلوث البيئة ويقضى على التنمية في تلك المناطق التي تحتاج إلى نظام معين في إدارة تلك الآبار.